JGP Journal of General Physiology

ARTICLE

Mechanotransduction by Membrane Proteins

Lack of evidence for participation of TMEM150C in sensory mechanotransduction

Julia Ojeda-Alonso[1], Valérie Bégay[1], Jonathan Alexis Garcia-Contreras[1], Andrea Fernanda Campos-Pérez[1], Bettina Purfürst[2], and Gary R. Lewin[1]

The membrane protein TMEM150C has been proposed to form a mechanosensitive ion channel that is required for normal proprioceptor function. Here, we examined whether expression of TMEM150C in neuroblastoma cells lacking Piezo1 is associated with the appearance of mechanosensitive currents. Using three different modes of mechanical stimuli, indentation, membrane stretch, and substrate deflection, we could not evoke mechanosensitive currents in cells expressing TMEM150C. We next asked if TMEM150C is necessary for the normal mechanosensitivity of cutaneous sensory neurons. We used an available mouse model in which the *Tmem150c* locus was disrupted through the insertion of a LacZ cassette with a splice acceptor that should lead to transcript truncation. Analysis of these mice indicated that ablation of the *Tmem150c* gene was not complete in sensory neurons of the dorsal root ganglia (DRG). Using a CRISPR/Cas9 strategy, we made a second mouse model in which a large part of the *Tmem150c* gene was deleted and established that these *Tmem150c*$^{-/-}$ mice completely lack TMEM150C protein in the DRGs. We used an ex vivo skin nerve preparation to characterize the mechanosenstivity of mechanoreceptors and nociceptors in the glabrous skin of the *Tmem150c*$^{-/-}$ mice. We found no quantitative alterations in the physiological properties of any type of cutaneous sensory fiber in *Tmem150c*$^{-/-}$ mice. Since it has been claimed that TMEM150C is required for normal proprioceptor function, we made a quantitative analysis of locomotion in *Tmem150c*$^{-/-}$ mice. Here again, we found no indication that there was altered gait in *Tmem150c*$^{-/-}$ mice compared to wild-type controls. In summary, we conclude that existing mouse models that have been used to investigate TMEM150C function in vivo are problematic. Furthermore, we could find no evidence that TMEM150C forms a mechanosensitive channel or that it is necessary for the normal mechanosensitivity of cutaneous sensory neurons.

Introduction

The search for genes coding for proteins that are necessary for touch-driven behavior was pioneered using *Caenorhabditis elegans* by Martin Chalfie and colleagues (Arnadóttir and Chalfie, 2010). These studies demonstrated how touch neurons transduce mechanical stimuli with a core mechanosensitive ion channel that works in the context of its interaction with several regulatory proteins that are themselves also necessary for mechanotransduction. Thus, the central MEC4/MEC10 ion channel conducts the ionic currents initiated by force (O'Hagan et al., 2005; Driscoll and Chalfie, 1991), but requires accessory proteins like MEC2 and MEC6 in order to function (O'Hagan et al., 2005; Goodman et al., 2002; Huang et al., 1995; Chelur et al., 2002; Brown et al., 2008). In recent years there has been considerable progress in identifying the molecules involved in force transduction by mammalian touch receptors. Thus, the MEC-2 like protein STOML3 was shown early on to be necessary for mammalian mechanoreceptors to transduce mechanical force into an electrical signal, a process we have termed sensory mechanotransduction (Wetzel et al., 2017, 2007). It is less clear whether mammalian orthologues of MEC4/MEC10 such as members of the acid sensing ion channel family (ASICs) participate directly in the transduction of mechanical force in sensory neurons (Omerbašić et al., 2014). The discovery of PIEZO1 and PIEZO2, very large membrane proteins that can

[1]Molecular Physiology of Somatic Sensation, Max Delbrück Center for Molecular Medicine in the Helmholtz Association, Berlin, Germany; [2]Electron Microscopy Core Facility, Max Delbrück Center for Molecular Medicine in the Helmholtz Association, Berlin, Germany.

Correspondence to Gary R. Lewin: glewin@mdc-berlin.de

J. Ojeda-Alonso's present address is Department of Neuroscience, Physiology and Pharmacology, University College London, London, UK. This work is part of a special issue on mechanotransduction by membrane proteins.

form homo-trimeric ion channels opened by mechanical force (Coste et al., 2010), raised the possibility that such proteins may participate in sensory mechanotransduction. There is now extensive evidence that *Piezo2* is genetically required for normal touch sensation in humans and mice (Chesler et al., 2016; Ranade et al., 2014; Murthy et al., 2018; Szczot et al., 2018; Hoffman et al., 2022). Indeed, conditional deletion of the *Piezo2* gene in mouse sensory neurons leads to the silencing of around half of all cutaneous mechanoreceptors (Ranade et al., 2014; Murthy et al., 2018), a phenotype that is almost identical to that observed in *Stoml3*$^{-/-}$ mice (Wetzel et al., 2017, 2007). Indeed, we have shown that STOML3 is a powerful regulator of PIEZO channel sensitivity to mechanical force (Poole et al., 2014a). Analysis of mice in which the *Piezo2* or *Stoml3* genes were ablated made it clear that the mechanosensitivity of many mechanoreceptors and almost all nociceptors relies on as yet unknown mechanosensitive ion channels. This fact has led many groups to search for further ion channel candidates that could confer mechanosensitivity to sensory neurons (Patkunarajah et al., 2020; Hong et al., 2016; Parpaite et al., 2021).

One early candidate sensory transduction channel was proposed to be the membrane protein TMEM150C, which has six predicted transmembrane domains (Hong et al., 2016). Subsequent studies suggested that the mechanosensitive currents identified after expression of TMEM150C in Hek293 cells were due to the confounding presence of endogenous PIEZO1 channels (Dubin et al., 2017; Anderson et al., 2018). However, one study provided evidence that TMEM150C might modulate the kinetics of PIEZO2 channel activation (Anderson et al., 2018). A recent publication using knock down approaches in the DRG also found no evidence that the *Tmem150c* gene contributes to mechanosensitive currents (Parpaite et al., 2021). The acquisition of mechanosensitivity by sensory neurons in the form of mechanosensitive currents is a developmentally regulated process occurring as soon as sensory axons reach their peripheral targets (Lechner et al., 2009). We had used this phenomenon to screen for the induction of genes encoding transmembrane proteins in sensory neurons coincident with the appearance of mechanosensitivity. One gene that was highly induced coincident with target innervation was *Tmem150c* (Herget, 2015), a finding that also prompted us to investigate the role of this gene in cutaneous mechanosensation. We generated mutant mice with *Tmem150c* gene ablation and examined these mice for sensory deficits. If TMEM150C is itself an ion channel or, like STOML3, a necessary modulatory subunit involved in sensory mechanotransduction, we would expect to find deficits in the physiology of cutaneous sensory neurons. Instead, after a detailed physiological evaluation of two mutant mouse models with an ablated *Tmem150c* locus, we conclude that there is no good evidence that this gene is involved in sensory mechanotransduction.

Materials and methods

Generation of the *Tmem150c* mutant mice and genotyping

Design and generation of guide RNAs used for targeting CRISPR/Cas9 region of *Tmem150c/Ttn3* locus in pronucleus of C57BL/6N, generation of founder mice and F1 heterozygous mice were performed by Ingenious Targeting Laboratory. Briefly, the following primers were used to amplify the wild-type (WT) allele (*Tmem150c* WT Rev1: 5′-TACCTGATGTATGGAGCATGCTTC-3′ and *Tmem150c* WT Fw1: 5′-TACTTTATAGCCGTGGAAGATGAC-3′) and the mutant allele (MEMT 1 Fw: 5′-CTCAATAACAGCCAC AAGGAAAG-3′ and MEMT 1 Rev: 5′-ACTGGCAGGGTTGTGTAA G-3′). F1 founders and F2 *Tmem150c*$^{+/-}$ mice were crossed with C57BL/6N mice. F3 and F4 heterozygous mice were mated to generate homozygous progenies used in the experiments. Progenies of heterozygous matings were born with Mendelian frequency that did not differ significantly from that expected (genotyped newborns n = 116; +/+ 25.9%: +/− 56%: −/− 18.1%).

Tmem150c KOMP line and genotyping

Tmem150c$^{+/LacZ}$ mice were generated from an ES cell clone created by international knockout mouse project (www.komp.org; Tate and Skarnes, 2011). The genotyping of the progenies were not performed according to KOMP protocol. Instead, the following primers were used to amplify a WT band (forward primer 5′-CACATTGGCAATCAGCATTACAC-3′ and reverse primer 5′-GTGCTGGGATCCTCCATTACC-3′), a part of the neomycin cassette (CDS-neoF 5′-GGGATCTCATGCTGGAGTTCT TCG-3′ and the above reverse), and a part of the LacZ cassette (LacZ-F 5′-ATCACGACGCGCTGTATC-3′ and LacZ-R 5′-ACA TCGGGCAAATAATATCG-3′).

RNA extraction and real-time PCR

Total RNA was isolated from tissues (epididymis, lumbal DRGs, and liver) using Relia prep RNA Tissue Miniprep System (Promega) according to the manufacturer's protocol. Total RNA was reverse transcribed at 42°C by using GoScript Transcription System (Promega) according to the manufacturer's protocol. Real-time PCR (RT-PCR) was run on a BioRad cycler. The following primers were used to amplify *Tmem150c* Ex4-Ex6 fragment (forward primer: 5′-GAAGCATGCTCCATACA-3′ and reverse primer 5′-CCAAGTAAGGTCATTCC-3′), Ex7–Ex8 fragment (forward primer: 5′-AGCTCACAAACGATGAA-3′ and reverse primer: 5′-CAGGATGAAATACAGGA-3′), and *Hprt1* fragment (forward primer: 5′-TCCTCCTCAGACCGCTTTT-3′ and reverse primer 5′-CCTGGTTCATCATCGCTAATC-3′).

X-gal staining

Tissues were dissected and quickly fixed in 2% PFA and 0.2% glutaraldehyde in 0.1 M sodium phosphate buffer for 3 h and postfixed with X-galactosidase (X-gal) fixative (0.2% glutaraldehyde, 100 mM $MgCl_2$, and 50 mM EDTA in PBS) for 20 min. Postfixed lumbar DRGs and epididymis were washed in PBS and cryoprotected in 30% sucrose overnight at 4°C. Tissues were embedded in OCT Tissue Tek (Sakura Finetek) on dry ice and stored at −80°C. Sections were cut at 12 µm using a Cryostat (Thermo Fisher Scientific) and X-gal staining was performed as previously described (Lobe et al., 1999). Briefly, sections were incubated in X-gal reaction buffer (5 mM potassium ferrocyanide, 5 mM potassium ferricyanide, 2 mM MgCl2, 0.02% Nonidet P-40, 0.01% sodium deoxycholate, and 0.5 mg/ml of X-gal in 100 mM sodium phosphate, pH 7.3) for 1 h (for epididymis) to

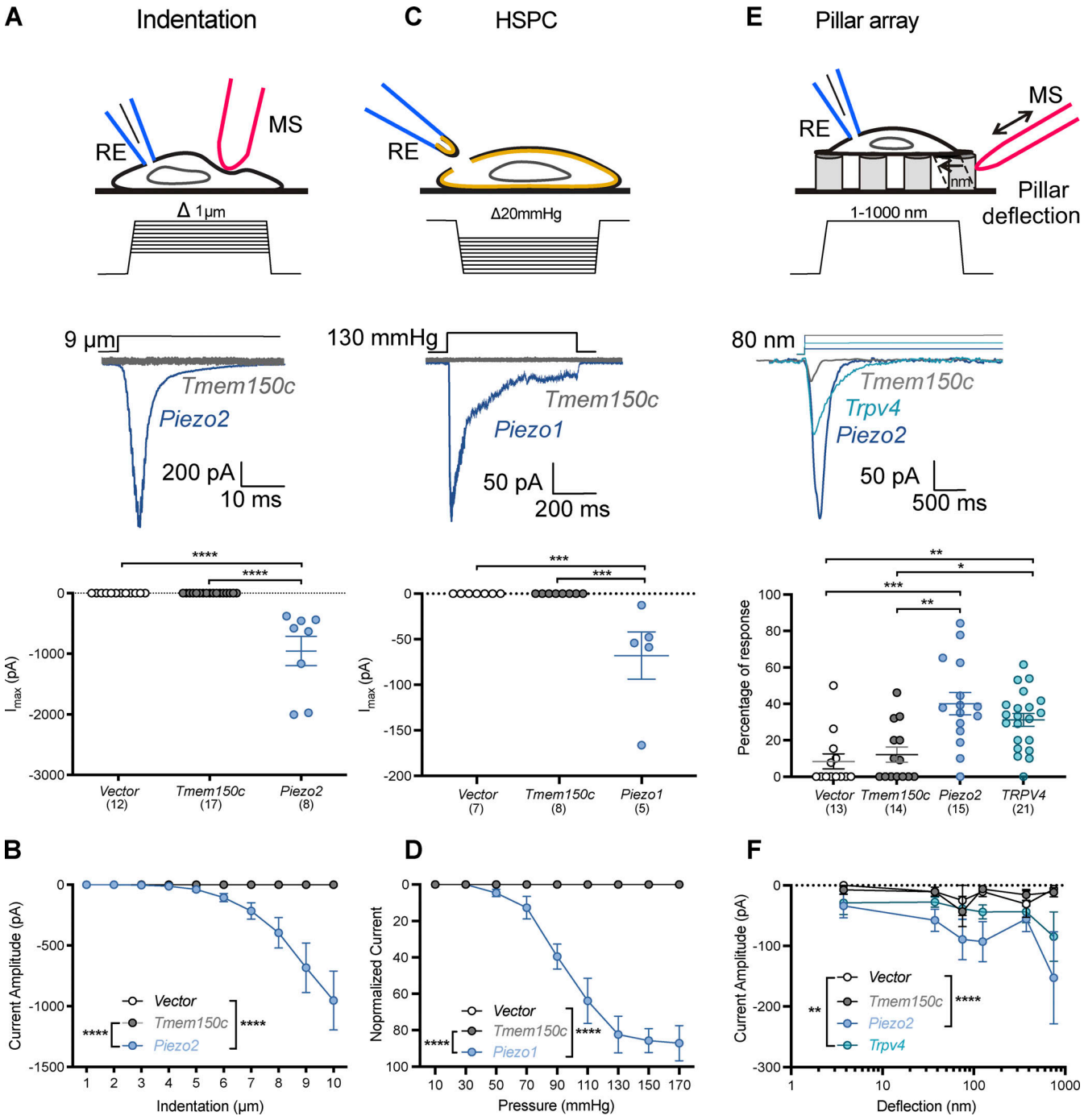

Figure 1. **Overexpression of TMEM150C in N2A$^{Piezo1-/-}$ cells does not evoke mechanosensitive currents. (A–C, and E)** Top: Cartoons of the different mechanical stimuli applied in this study together with representative traces from mechanosensitive currents evoked using indentation (A), HSPC (C), or pillar arrays (E) methods. *Piezo* and *Trpv4* were used as positive controls. Cells overexpressing *Tmem150c* did not display mechanosensitive currents in any of the assays that differed from cells transfected with the empty expression vector. RE, recording electrode; MS, mechanical stimulator. A, C, and E quantified for all stimulus strengths in B, D, and F. **(A and B)** Scatter plots showing the maximal peak (Imax) from mechanosensitive currents observed in N2a$^{Piezo1-/-}$ cells transfected with vector, *Tmem150c* or *Piezo2*. No mechanosensitive currents were observed for N2A$^{Piezo1-/-}$ transfected with *Tmem150c* (Kruskal–Wallis test, *Tmem150c* vs. vector P > 0.9999; *Piezo2* vs. vector, P < 0.0001; *Piezo2* vs. *Tmem150c* P < 0.0001) with indentation (A and B) or HSPC (C and D); Kruskal–Wallis test, *Tmem150c* vs. vector P > 0.9999; *Piezo1* vs. vector P = 0.0003; *Piezo1* vs. *Tmem150c* P = 0.0002. **(E)** N2A$^{Piezo1-/-}$ cells transfected with vector controls occasionally displayed a pillar induced mechanosensitive current, but the frequency of such currents was not higher in cells expressing *Tmem150c*. In contrast, almost all cells overexpressing either *Piezo2* or *Trpv4* showed large and robust mechanosensitive currents to pillar deflection, Kruskal–Wallis test, *Tmem150c* vs. vector P > 0.9999; vector vs. *Piezo2* P = 0.0007; vector vs. *Trpv4* P = 0.003; *Tmem150c* vs. *Piezo2* P = 0.002; *Tmem150c* vs. Trpv4 P = 0.01. **(E and F)** Current kinetics observed in N2A$^{Piezo1-/-}$ overexpressing a vector, *Tmem150c* or *Piezo2* channels. Left: Indentation–current amplitude relationship (A) showing that *Tmem150c* is indentation-insensitive. Two-way ANOVA, *Piezo2* vs. vector, P < 0.0001; *Piezo2* vs. *Tmem150c* P < 0.0001. **(C and D)** Overexpression of *Tmem150c* was not associated with the pressure activated currents in membrane patches subjected to pressure pulses. Two-way ANOVA, *Piezo2* vs. vector, P < 0.0001;

Piezo2 vs. *Tmem150c* P < 0.0001. Current amplitude–deflection relationship (I) for currents recorded in cells expressing *Tmem150c*, *Piezo2*, or *Trpv4*. **(F)** Cells expressing *Tmem150c* exhibited similar amplitude–deflection currents as cells transfected with the empty vector. Two-way ANOVA, *Tmem150c* vs. vector P > 0.9999; vector vs. *Piezo2* P = 0.0003; vector vs. *Trpv4* P = 0.0136. *P ≤ 0.05, **P > 0.01, ***P < 0.001, ****P < 0.0001.

overnight (DRGs) at 37°C. Sections were washed in PBS and counter stained with nuclear fast-red (N8002; Sigma-Aldrich). Sections were observed and captured on a Leica DM 5000 B microscope (Leica).

Immunoblotting

Tissues from *Tmem150c*$^{-/-}$ mutants and WT mice were lysed with 8 M urea buffer and protein concentrations were determined using the Bradford reagent (Sigma-Aldrich). Proteins were separated by SDS-PAGE, followed by Western blotting using rabbit antibody against the C-terminal part of TMEM150C (ABN2266; Millipore), mouse β-actin (A1978; Sigma-Aldrich), and horseradish-peroxidase–conjugated secondary antibodies (111-035-003; Jackson ImmunoResearch), and chemiluminescence detection (Thermo Fischer Scientific).

Electron microscopy

The general procedure followed for the quantification of peripheral nerves was described by Smith et al. (2012). Tibial nerves from 30-wk-old *Tmem150c*$^{-/-}$ mice and WT littermates were analyzed. Nerves were freshly isolated and fixed in 4% paraformaldehyde/2.5% glutaraldehyde in 0.1 M phosphate buffer for at least 24 h at 4°C. After treatment with 1% OsO_4 for 2 h, each nerve was dehydrated in a graded ethanol series and propylene oxide and embedded in polyresin. Nerves were cut using a microtome in semi-thin (1 µm) and ultrathin sections (70 nm). Semi-thin sections were stained with toluidine blue and ultrathin sections were contrasted with uranyl acetate and lead acetate. Semi-thin sections were examined in a light microscope to determine the total number of myelinated axons within the nerve. Ultrathin sections were examined with a Zeiss 910 electron microscope and images were taken at an original magnification of 2,500×. 15 pictures (22.5 × 14.9 µm) per ultrathin section from each nerve from three adult WT and *Tmem150c*$^{-/-}$ mice were analyzed. Using iTEM software, the C:A-fibers ratio, the myelin thickness and g-ratio of the myelin sheath of A-fibers, were determined. The g-ratio is defined as the ratio of the inner axonal diameter to the total outer diameter of the myelin sheath.

Based on the C:A-fibers ratio determined in ultrathin sections, the total number of C-fibers within the nerve was extrapolated to the number of A-fibers of each semi-thin section. To further compare between different animals, the total number of myelinated and unmyelinated axons was extrapolated to the smallest nerve area.

Cell culture and transfection

DNA plasmids that contain mouse *Tmem150c*, *mouse Piezo1*, and *mouse Piezo2* sequences were obtained using large-scale bacterial culture (200 ml maxi-prep). Single colonies from transformed bacteria were picked into LB medium containing ampicillin or kanamycin and grown overnight at 37°C with shaking. The maxi-preps were carried out according to the manufacture's protocol. Plasmid DNA was diluted in water and the DNA concentration was measured using the NanoDrop2000 spectrophotometer (Thermo Fisher Scientific).

N2a cells from mice were used. N2a cells present endogenous mechanically gated currents due to the expression of Piezo1. For that reason, in most of the experiments N2a cells where *Piezo1* was deleted (N2a-P1KO) via CRISPR/Cas9 technology were used (Moroni et al., 2018). Cells were plated onto PLL glass coverslips or PLL covered pillar arrays in medium without serum and let them attach for at least 4 h. For the transfection, 1 µg of DNA was mixed with 3 µl of FuGeneHD and 300 µl of OptiMem. After 15 min of incubation at room temperature, the mixture was added to each well. Cells were incubated at 37°C in 5% CO_2 overnight. Efficiently transfected cells could be detected by a fluorescent marker signal at least 24 h after transfection.

Whole-cell electrophysiology

Whole-cell recordings in voltage clamp were performed from the N2A cell line *Piezo1* knockout. Patch pipettes were pulled from borosilicate glass with a tip resistance of 3–5 MΩ were filled with intracellular solution (in mM): 100 KCl, 10 NaCl, 1 $MgCl_2$, 10 HEPES, and pH adjusted to 7.3 with KOH. The extracellular solution contained (in mM): 140 NaCl, 4 KCl, 1 $MgCl_2$, 2 $CaCl_2$, 4 glucose, and 10 HEPES. Cells were clamped to a holding potential of −60 mV. Recordings were made using an EPC-10 amplifier (HEKA) with Patchmaster and Fitmaster software (HEKA). Pippette and membrane capacitance were compensated using the auto function of Patchmaster and series resistance was compensated by 70% to minimize voltage errors.

Indentation

Mechanically activated currents were recorded as described earlier (Hu and Lewin, 2006; Wetzel et al., 2007). The mechanical probe consisted of fire-polished glass pipette (tip size 2–3 µm) was manipulated by a piezo-driven micromanipulator (Nanomotor MM3A; Kleindiek Nanotechnik). Calibration of a single-step size was achieved moving a large number of steps and measuring the distance, repeated three times. Motor's velocity of movement was set at 3.5 µm/ms. The voltage signal sent to the nanomotor by the control unit was simultaneously monitored by a second channel at the EPC10 amplifier, allowing to measure the delay between the nanomotor movement and mechanically activated current, or latency. The probe was positioned at 60° near to the cell body and movements of the mechanical probe were executed in the in/out axis of the device (axis C) for 300–500 ms with 500 ms pause in between steps. A voltage divider box (MM3-LS trigger, Kleindiek Nanotechnik) was connected that provided analog voltage output signal corresponding to the piezo signals. Depending on the movement of the piezo micromanipulator, the voltage signal was registered as small pulse or just a change in a DC voltage. Only the somas were

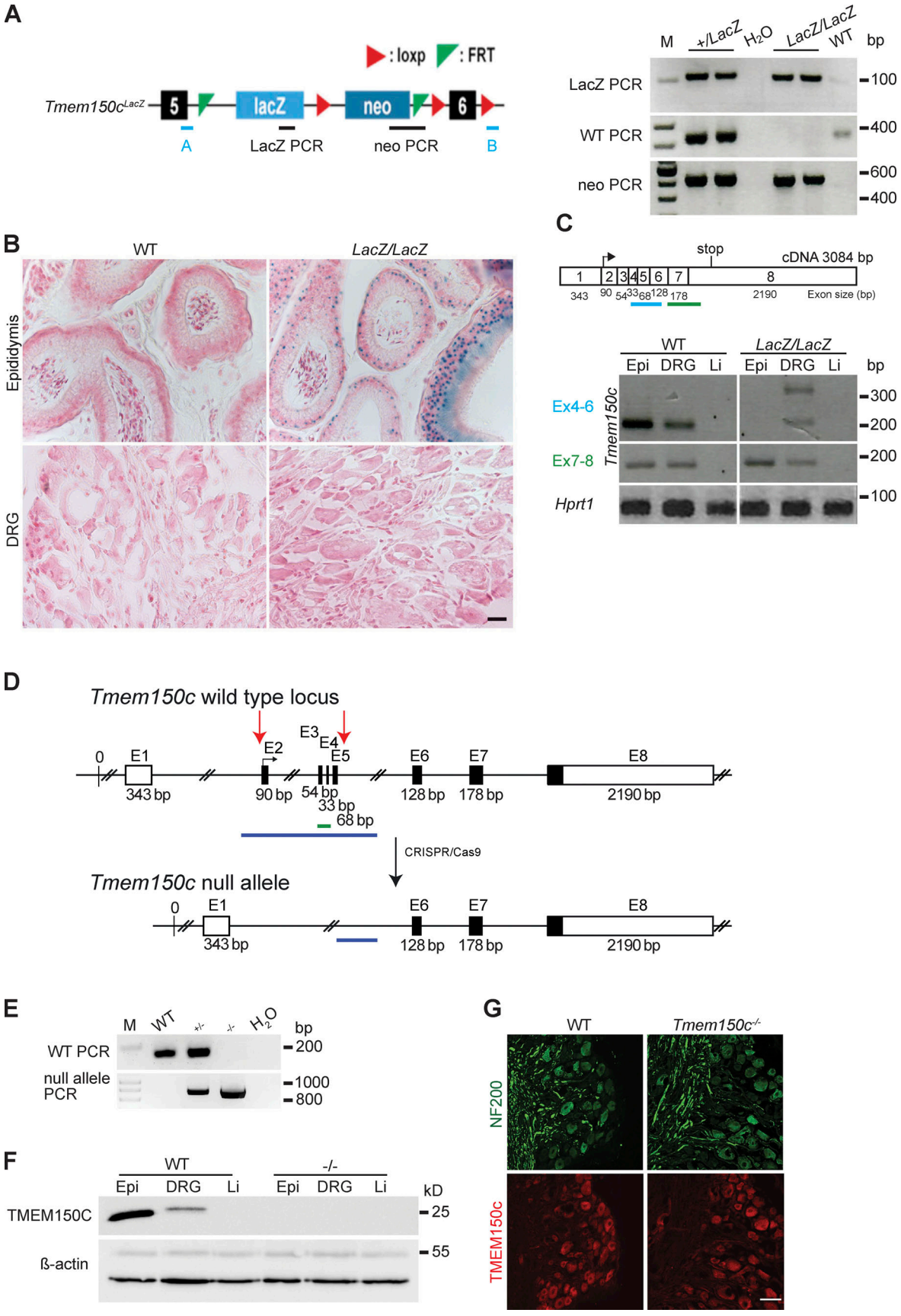

Figure 2. **Generation and characterization of *Tmem150c* mouse models. (A)** Left: Schematic representation of *Tmem150c* locus of the knockout first mouse (*Ttn3*^{LacZ}), named here *Tmem150c*^{LacZ}, generated by the trans-National Institutes of Health Mouse initiative knockout Mouse project (https://www.komp.org)

containing a LacZ cassette and a neomycin cassette with a stop codon inserted between exons 5 and 6 and resulting in a frame shift. Right: Representative gels showing PCR results for neomycin cassette, LacZ cassette, and WT bands. A and B primers (in blue) used for the amplification of the WT band. Genomic DNA from ear biopsies from WT, heterozygous, and homozygous mice were analyzed. M: DNA marker. **(B)** β-galactosidase staining (blue) of epididymis (positive tissue control) and DRG of *Tmem150c*$^{LacZ/LacZ}$ mice. Note the unexpected lack of staining in the DRGs of *Tmem150c*$^{Lacz/LacZ}$ mice. WT tissues used as negative control. Scale bar = 20 µm. **(C)** Top: Schematic representation of *Tmem150c* cDNA (source ensemble Tmem150c-201) containing 8 exons (1–8) with the start codon located in exon 2 (2) and the stop codon located in exon 8 (8). Bottom: RT-PCR performed on cDNA prepared from tissues of WT mice and *Tmem150c*$^{Lacz/LacZ}$ mice with the blue line indicating amplicon covering exon 4–6 (the targeted area of *Tmem150c*^{LacZ} allele) and the green line indicating amplicon covering the end of exon 6 to the beginning of exon 8. Note the presence of unexpected bands in DRG of the *Tmem150c*$^{Lacz/LacZ}$ mice but the absence of bands in Epi and Li as expected. *Hprt1* (housekeeping gene) is used as positive control for all tissues. Epi, epididymis (positive control); Li, liver (negative control). **(D)** Schematic representation of *Tmem150c* null allele generation using CRISPR/Cas9 technology: deletion of nucleotide sequence between the end of intron 1–2 and the beginning of intron 5–6. WT allele and null allele are shown: exon1 (E1) encodes the 5′ UTR and E8 the 3′ UTR (white box). Black box: coding sequence. (source ensemble ENSMUSG00000005064017). Red arrows indicate the location of gRNA sequences used for CRISPR/Cas9. **(E)** PCR performed on genomic DNA from ear biopsies from WT, heterozygous, and homozygous mice are shown. The WT amplicon is represented by the green line in the scheme covering E3 and E4 (179 bp). The null allele amplicon is represented by the blue line producing an 886 bp fragment when the nucleotide sequence between intron 1–2 and intron 5–6 (3,039 bp in WT) is deleted as in the null allele. Note that this PCR fragment could amplify a 3,039 bp fragment in WT mice (see blue line), but this is not possible using the chosen PCR conditions. M: DNA marker. **(F)** TMEM150C protein expression using Western blot showing absence of TMEM150C protein in tissues from *Tmem150c*$^{-/-}$ mice. Epididymis (Epi, positive control) and liver (Li, negative control). β-actin was used as loading control. **(G)** Immunostaining performed on DRGs from WT and *Tmem150c*$^{-/-}$ mice using an antibody directed against the C-terminal part of TMEM150C (same as in F). Note that TMEM150C antibody labeled neurons in WT, but also in *Tmem150c*$^{-/-}$ mice. NF200 was used to label myelinated neurons. Scale bar = 50 µm. Source data are available for this figure: SourceData F2.

stimulated, the evoked currents were recorded with a sampling frequency of 200 kHz.

High-speed pressure clamp

High-speed pressure clamp (HSPC) recordings were performed in excised outside-out patches pulled from N2a cells at room temperature. Recording pipettes were prepared using a DMZ puller and subsequently polished to a final resistance of 6–8 MΩ for outside-out patches. Currents were elicited by negative pressure stimuli, with an Ala Instrument device, applied through the recording pipette holding at −60 mV. A protocol of pressure steps from 10 to 150 mmHg in 20 mmHg steps during 600 ms was used. Uncompensated series resistance values were <2 MΩ. The recorded currents responsive to the pressure curve from each cell were fitted to a Boltzmann equation using the FitMaster program (HEKA, Elektronik GmbH).

Table 1. **Proportions and conduction velocities of sensory afferents recorded from *Tmem150c*$^{LacZ/LacZ}$ from saphenous skin-nerve preparation**

	Tmem150c$^{+/+}$	*Tmem150c*$^{LacZ/LacZ}$
Aβ-fibers RAM CV (m/s)	13.4 ± 0.6 (29)	14.4 ± 0.9 (22)
t test	P = 0.54	
SAM CV (m/s)	16.6 ± 0.9 (24)	15.1 ± 0.7 (31)
t test	P = 0.23	
Aδ-fibers DH CV (m/s)	4.6 ± 0.3 (19)	6.2 ± 0.5 (12)
t test	P = 0.04	
AM CV (m/s)	4.8 ± 0.5 (23)	4.6 ± 0.5 (27)
t test	P = 0.83	
C-fibers CV (m/s)	0.93 ± 0.16 (10)	0.89 ± 0.12 (12)
t test	P = 0.89	
Total number	105	104

Mean values ± SEM are shown. Data set from *Tmem150c*$^{+/+}$ mice were compared to those fibers recorded from mutant *Tmem150c*$^{LacZ/LacZ}$ mice using a Student's *t* test. Related to Fig. S1.

Pillar arrays

Pillar arrays were prepared as previously described (Patkunarajah et al., 2020; Poole et al., 2014a; Servin-Vences et al., 2017). Briefly, silanized negative masters were used as templates. Negative masters were covered with poly-dimethylsilozane (PDMS; syligard 184 silicone elastomer kit, Dow Corning Corporation) mixed with a curing agent at 10:1 ratio. After 30 min, glass coverslips (thickness 2) were placed on the top of the negative masters containing PDMS and the coated master placed at 110°C for 1 h. After curing, the pillar array was peeled away from the master. The resulting radius- and length-size of individual pilus within the array was 1.79 and 5.8 µm, respectively. While the elasticity and the spring constant of each pilus was 2.1 MPa and 251 pN-nm, respectively, as previously reported (Patkunarajah et al., 2020; Poole et al., 2014a; Servin-Vences et al., 2017). Before use, pillar arrays were activated by plasma cleaning and coated with PLL (Deiner Electronic GmbH) and cells were allowed to attach.

To generate quantitative data, an individual pilus subjacent to a cell was deflected using a heat-polished borosilicate glass pipette (~2 mm in diameter) driven by a MM3A micromanipulator (Kleindiek Nanotechnik) as described in Poole et al. (2014a) and Servin-Vences et al. (2017). Pillar deflection stimuli were applied in the range of 0–1,000 nm, and the electrical response of the cells was monitored using whole-cell patch-clamp. A bright-field image (Zeiss Axio Observer A1 inverted microscope) was taken before, during, and after pillar deflection stimuli using a 40× objective and a CoolSnapEZ camera (Photometrics). The pillar movement was calculated comparing the light intensity of the center of each pilus before and after the stimuli with a 2-D–Gaussian fit (Igor Software, WaveMetrics).

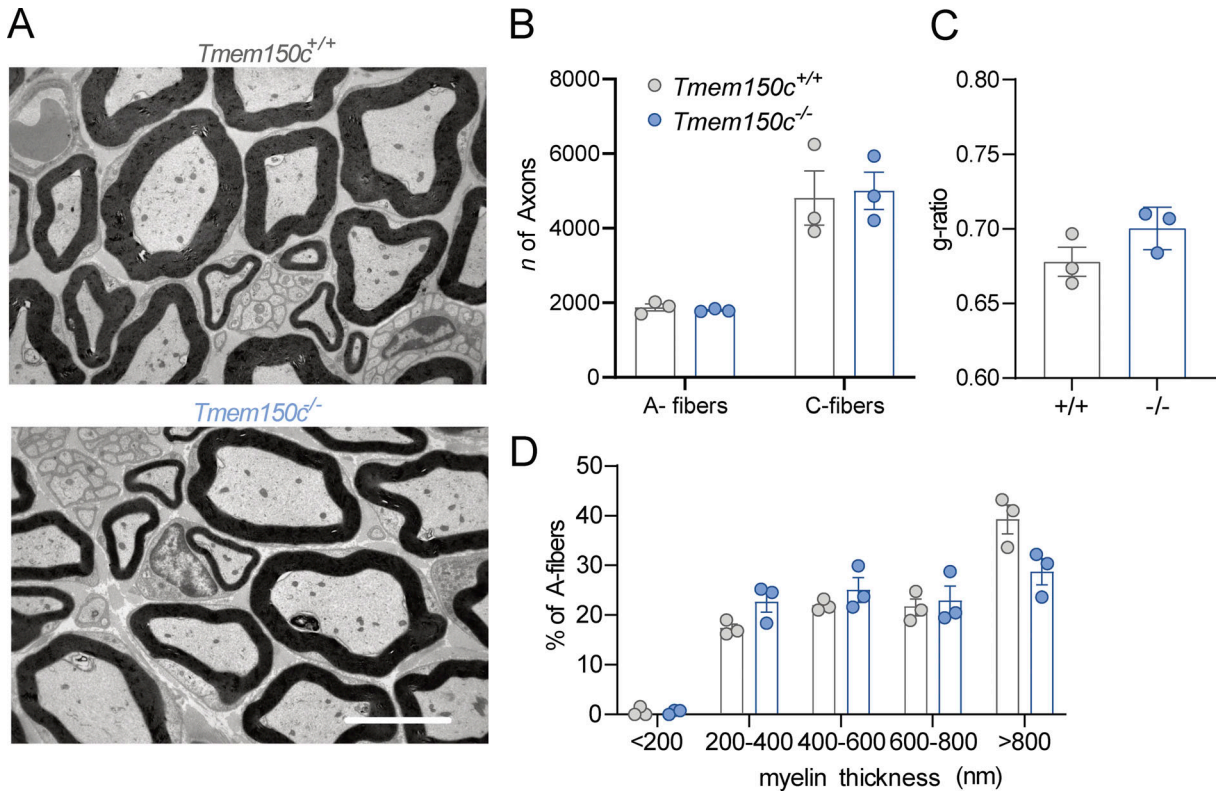

Figure 3. **Ultrastructural analysis of the tibial nerve. (A)** Example electronmicrographs from the tibial nerve of a WT *Tmem150c*$^{+/+}$ (top) and *Tmem150c*$^{-/-}$ mouse (bottom). Scale bar = 5 µm. **(B)** Quantification of axon numbers revealed no loss of myelinated A-fibers (two-way ANOVA, P = 0.99) or unmyelinated C-fibers (two-way ANOVA, P = 0.95). **(C)** Measurements of the G-ratio a measure of myelin thickness showed no difference between genotypes (unpaired *t* test, P = 0.16). **(D)** Quantification of myelin thickness across all axon sizes (binned by myelin thickness) revealed no statistically significant differences between nerves taken from control *Tmem150c*$^{+/+}$ (grey) and *Tmem150c*$^{-/-}$ mice (blue; two-way ANOVA, P = 0.92 for genotype), means ± SEM.

Extracellular recording from tibial nerve

Electrophysiological recordings from cutaneous sensory fibers of the tibial nerve were made using an ex vivo skin nerve preparation following the method described previously (Walcher et al., 2018; Wetzel et al., 2007). Briefly, the animal was sacrificed by cervical dislocation, and the hair of the limb was shaved off. The glabrous skin from the hind paw was removed along with the tibial nerve dissected up to the hip and cut. The glabrous skin along with the tibial nerve still attached to the hindpaw was transferred to a bath chamber which was constantly perfused with warm (32°C) oxygen-saturated interstitial fluid. The remaining bones, muscle, and ligament tissue were gently removed as much as possible, allowing the glabrous skin and tibial nerve preparation to last at least 6 h of recording in a healthy, stable condition in an outside-out configuration. The tibial nerve was passed through a narrow channel to an adjacent recording chamber filled with mineral oil.

Single-unit recordings were made as previously described (Walcher et al., 2018; Wetzel et al., 2007). Fine forceps were used to remove the perineurium and fine nerve bundles were teased and placed on a platinum wire recording electrode. Mechanical sensitive units were first located using blunt stimuli applied with a glass rod. The spike pattern and the sensitivity to stimulus velocity were used to classify the unit as previously described (Walcher et al., 2018; Wetzel et al., 2007). Raw data were recorded using an analog output from a Neurolog amplifier, filtered, and digitized using a Powerlab 4/30 system and Labchart 8 software with the spike-histogram extension (ADInstruments Ltd.). All mechanical responses analyzed were corrected for the latency delay between the electrical stimulus and the arrival of the action potential at the electrode. The conduction velocity (CV) was measuring the formula CV = distance/time delay, in which CVs > 10 ms^{-1} were classified as RAMs or SAMs (Aβ, <10 ms^{-1} as Aδ and <1 ms^{-1} as C-fibers).

Mechanical stimulation

Mechanical stimulation of the receptive field of the recorded fibers was performed using a piezo actuator (P-602.508; Physik Instrumente) connected to a force-measurement device (Kleindiek Nanotechnik, PL-FMS-LS). Different mechanical stimulation protocols were used to identify and characterize the sensory afferents. Mechanoreceptors were tested with a vibrating stimulus with increasing amplitude and 20 Hz frequency. The force needed to evoke the first action potential was measured. Additionally, a ramp and hold step was used with constant force (100 mN) and repeated with varying probe movement velocity (0.075, 0.15, 0.45, 1.5, and 15 mm s^{-1}). Only the firing activity evoked during the dynamic phase was analyzed. SAM mechanoreceptors and nociceptors were tested with a mechanical stimulus with a constant ramp (1.5–2 mN ms^{-1}) and increasing

Table 2. **Proportions and conduction velocities of primary afferents recorded from *Tmem150c*$^{-/-}$ compared to *Tmem150c*$^{+/+}$ mice**

	Tmem150c$^{+/+}$	*Tmem150c*$^{-/-}$
Aβ-fibers RAM CV (m/s)	14.3 ± 0.7 (20)	12.3 ± 0.48 (24)
t test	P = 0.24	
SAM CV (m/s)	12.4 ± 0.4 (26)	11.8 ± 0.3 (32)
t test	P = 0.20	
Aδ-fibers DH CV (m/s)	7.1 ± 0.4 (16)	6.9 ± 0.3 (18)
t test	P = 0.78	
AM CV (m/s)	5.3 ± 0.5 (16)	3.9 ± 0.4 (25)
t test	P = 0.04	
C-fibers CV (m/s)	0.55 ± 0.05 (26)	0.64 ± 0.06 (24)
t test	P = 0.21	
Total number	104	123

Student's *t* test was used to test for differences between recordings made from WT and *Tmem150c*$^{-/-}$ mice.

force amplitude, spikes evoked during the static phase were analyzed.

Gait analysis

Gait analysis was carried out using the "mouse walk" method described by Mendes et al., (2015). An acrylic walkway 80 cm in length was produced with white-light LED strips attached to its sides. Another similar walkway was used as a background light (sky) with white plastic attached to the top to provide a lighter and even background. These two walkways were embedded in a black custom-built rack with a mirror angled 45° below the walkway. On the left side of the walkway a small custom-built Plexiglas house was introduced to provide shelter for the animals. A monochromatic high-speed camera (FLIR, RoHS 2.3 MP Mono Grasshopper) was used to videotape the animal's walk (the mirror image/reflection was recorded). Experiments were performed with no additional light source present in the room. Animals were initially habituated to the walkway for 15 min—they were put in the setup on the right side, opposite of the shelter and allowed to explore freely. Usually, they spent most of the time in the shelter after the initial exploration of the walkway. At the end of the habituation time the shelter containing the animal was removed, the animal was placed on the right side again and the shelter placed on the left side—to make the animal cross the walkway a few times. Each animal was recorded multiple times to obtain recordings with constant velocity and no stops during the crossing—four to five of these videos were then cropped, converted to single image stacks (every frame was converted into one image, the framerate of the camera was 150 frames/s) and analyzed using a MATLAB script provided by Cesar Mendes (iNOVA4Health, NOVAMedical School, Faculdade de Ciências Médicas, Universidade Nova de Lisboa, Lisboa, Portugal). The white LED light transilluminates the walkway creating an effect called fTIR (frustrated total internal reflection)—in brief, the light traveling through the walkway is reflected differently when there is contact of the animals' paw with the walkway. This is visualized through lighting of the contact area—the intensity of the reflected footprint is increasing with pressure/weight. This was used for the annotation of the videos, the paws as well as the head, nose, center of the body, and other markers were used to evaluate ∼26 parameters of the animals' gait.

Online supplemental material

Fig. S1 shows the results of the electrophysiological analysis of mechanoreceptors and nociceptorss from the Saphenous nerve of *Tmem150c*$^{Lacz/LacZ}$ mice.

Results

Initial reports suggested that heterologous expression of *Tmem150c* is associated with the appearance of mechanosensitive currents in Hek293 cells to indentation (Hong et al., 2016). Mechanosensitive currents can be measured using a variety of different methods to apply mechanical force. The most commonly used method is to poke cells that express the proteins of interest, but currents can also be evoked by applying fast pressure pulses to patches of membranes in cell attached mode (Taberner et al., 2019) or in excised outside-out patches (Moroni et al., 2018). In addition, some ion channels such as TRPV4 and PIEZO2 are not efficiently gated by membrane stretch, but are activated by displacement of the extracellular matrix underneath cells expressing the channel protein (Poole et al., 2015; Servin-Vences et al., 2017). Here, we expressed *Tmem150c* in N2A cells in which the *Piezo1* gene had been ablated (N2A$^{Piezo1-/-}$ cells; Moroni et al., 2018) and evaluated whether mechanosensitive currents could be evoked with all three of the methods described above. In agreement with studies using Hek293 cells lacking PIEZO1, we found no poking-induced currents in N2A$^{Piezo1-/-}$ cells transfected with a *Tmem150c* cDNA similarly to the vector control (Fig. 1, A and B). In contrast, in all cells recorded expressing WT *Piezo2* we could measure robust poking-induced currents, the amplitudes of which increased with increasing indentation strength (Fig. 1, A and B). Similarly, we could record robust inward currents in outside out excised patches to fast pressure pulses taken from N2A$^{Piezo1-/-}$ cells expressing *Piezo1*, but could measure no currents in patches taken from cells transfected with *Tmem150c* expression constructs or vector transfected control cells (Fig. 1, C and D). Finally, we plated N2A$^{Piezo1-/-}$ cells on elastomeric pillar arrays and evaluated whether pili movement could evoke mechanosensitive currents in cells expressing *Tmem150c*. As a positive control we used cells expressing *Trpv4* or *Piezo2* in which we could measure robust inward currents to pili deflections in a range from 5 to 1,000 nm. In contrast, we could measure no deflection-induced current from cells expressing *Tmem150c* (Fig. 1, E and F). We conclude that TMEM150C by itself is unlikely to form a membrane channel that can be gated by force applied through membrane stretch or through extracellular matrix.

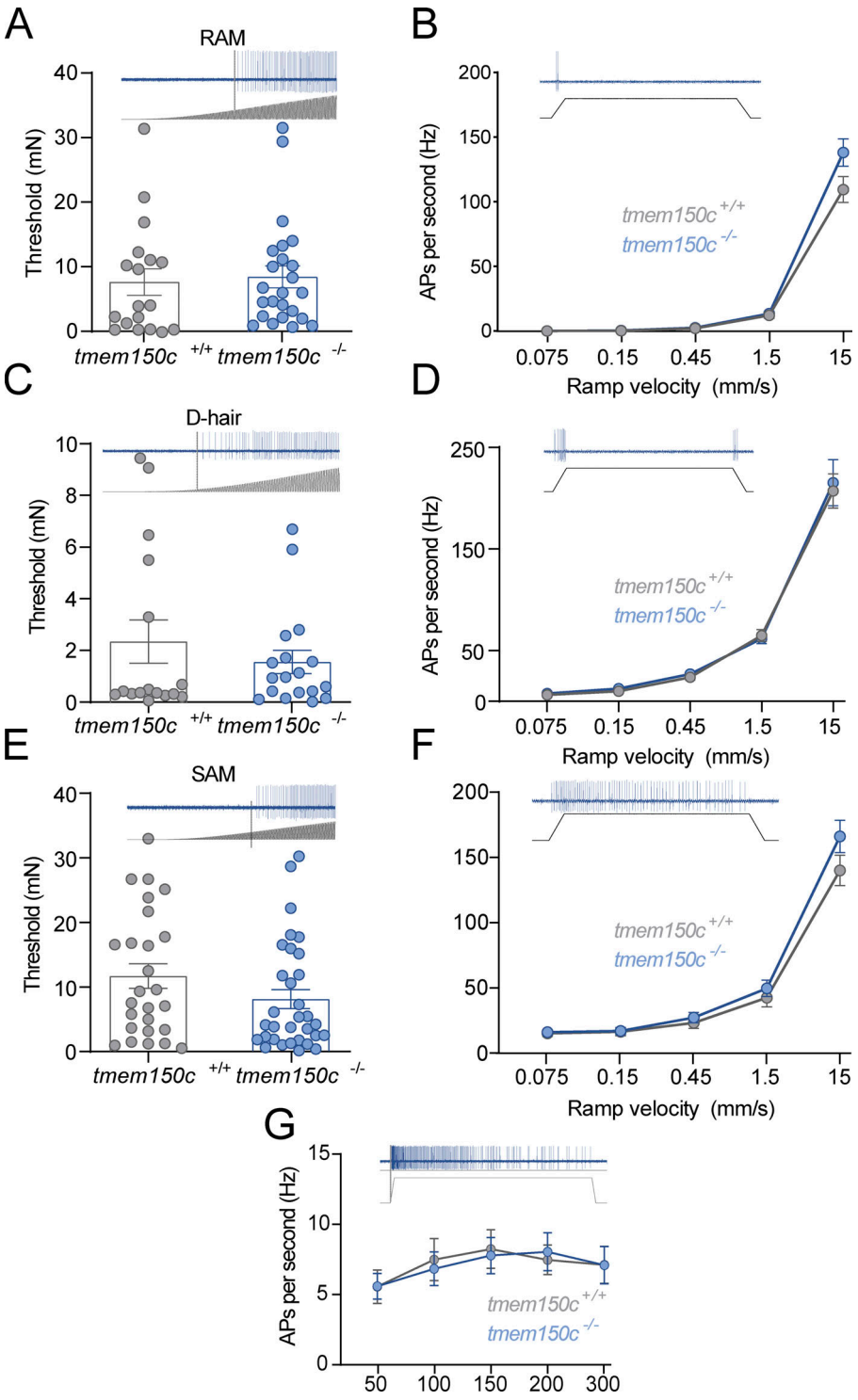

Figure 4. **Low threshold mechanoreceptors are unchanged in *Tmem150c*$^{-/-}$ mice. (A and B)** Rapidly adapting mechanoreceptors were stimulated with a linearly increasing 20 Hz sinusoidal force stimulus to determine mechanical threshold in mN (A) or a series of ramp and hold stimuli of different velocities (B; example recordings shown). There was no difference in these mean parameters in RAMs recorded from *Tmem150*$^{-/-}$ mice compared to littermate controls (*Tmem150c*$^{+/+}$ mice; Mann-Whitney U-test, P = 0.40 for threshold; two-way ANOVA, P = 0.07 for stimulus response). **(C and D)** D-hair mechanoreceptors were also probed with the same quantitative stimuli. There was no difference in the mean mechanical threshold (Mann-Whitney test, P = 0.74) or velocity sensitivity of D-hair mechanoreceptors between the two genotypes (two-way ANOVA, P = 0.70). **(E–G)** SAMs were also probed with the same quantitative stimuli (E and F), as well as a series of 10 s long ramp and hold stimuli of increasing holding force (50–300 mN; G). There was no statistical difference in the mean mechanical threshold (Wilcoxin signed ranks, P = 0.06), velocity sensitivity (two-way ANOVA, P = 0.27), or stimulus response function of SAMs (two-way ANOVA, P = 0.95) between the two genotypes (G). The numbers of fibers included in the analysis can be found in Table 2. All means ± SEM.

Hong and colleagues used a mouse model in which the *Tmem150c* gene had been ablated using the Knockout-first strategy (Tate and Skarnes, 2011). They recorded fewer mechanosensitive currents with slowly inactivating properties in *Tmem150c* mutant sensory neurons compared to controls (Hong et al., 2016). We obtained the same mouse mutant strain, but derived from a different ES cell clone, to evaluate the function of TMEM150C in somatosensory neurons. In these mice a β-galactosidase cassette (LacZ) with a splice acceptor was inserted between exon 5 and 6 which should lead to the production of an aberrant truncated transcript encoding a LacZ reporter (Fig. 2 A). We thus named this allele *Tmem150c*^{lacZ} (named *Ttn3*^{LacZ} in Hong et al., 2016) and subsequently generated homozygous *Tmem150c*$^{LacZ/LacZ}$ on a C57BL/6N background together with WT littermate controls (Fig. 2, A–C). There was no indication that *Tmem150c*$^{LacZ/LacZ}$ mice showed embryonic or post-natal lethality and homozygous mice appeared normal and healthy. Since the TMEM150C

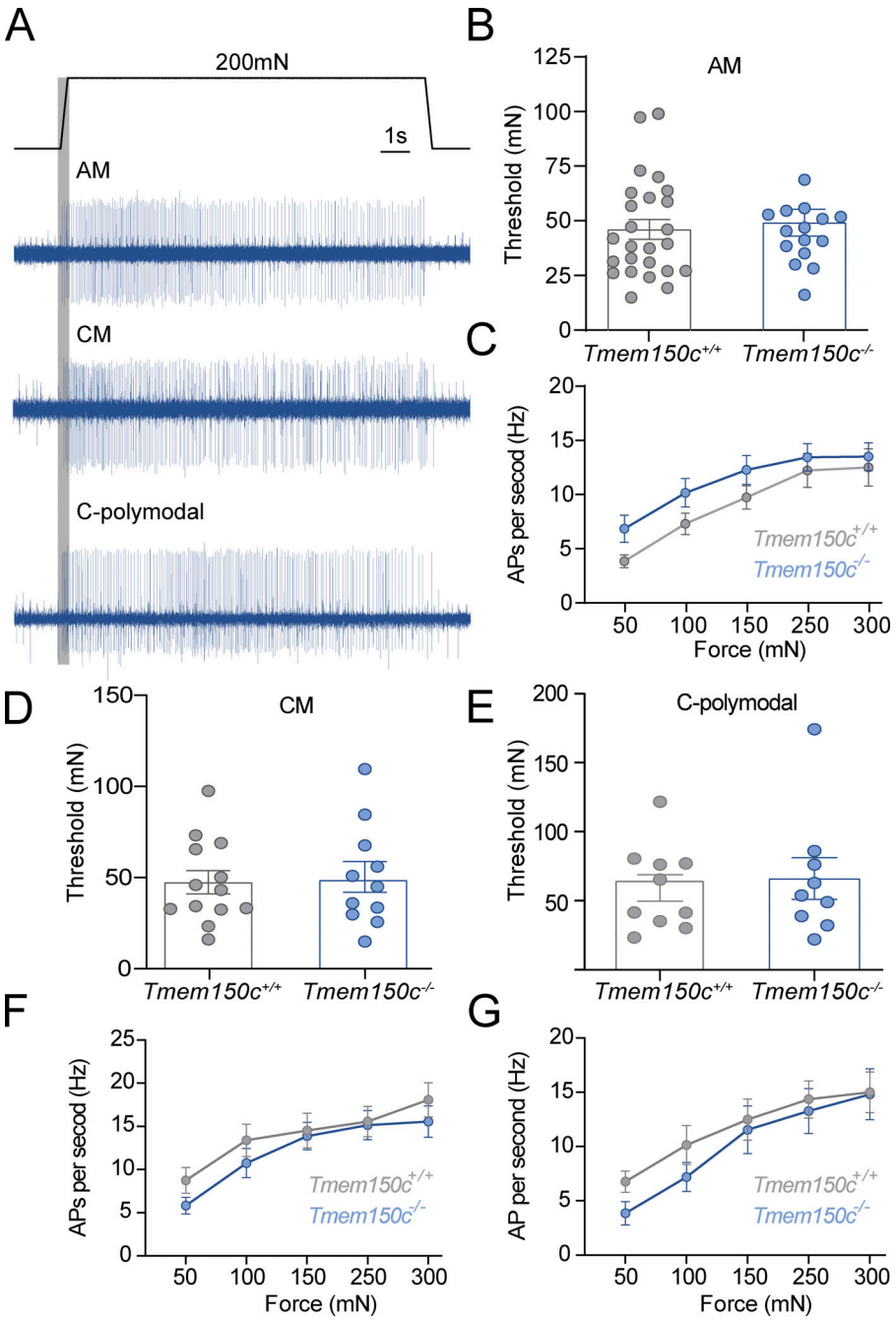

Figure 5. **The mechanosensitivity of nociceptors was unchanged in *Tmem150*$^{-/-}$ mice.** We recorded from thinly myelinated mechanonociceptors termed A-mechanonociceptors (AM), C-fiber mechanonociceptors (CM), and polymodal C-fiber nociceptors, the latter respond to mechanical stimuli and at least one other stimulus modality like heat or cold. **(A)** Example recordings from these three receptor types in response to a ramp and hold controlled force stimuli. Mechanical thresholds were measured as the force required to evoke the first spike during the stimulus ramp phase. **(B)** For AMs, there was no difference in the mean mechanical threshold between fibers recorded from *Tmem150*$^{-/-}$ mice compared to littermate controls (*Tmem150c*$^{+/+}$ mice; Mann-Whitney U-test, P = 0.95). **(C)** Stimulus response properties of AMs to controlled force stimuli were also not different between genotypes (two-way ANOVA, P = 0.20). **(D and E)** The mean mechanical thresholds of CMs and C-polymodal fibers did not differ between genotypes (CMs unpaired *t* test, P = 0.90; C-polymodal Mann-Whitney U-test, P = 0.99). **(F and G)** The stimulus response functions of CM and C-polymodal fibers also did not differ between genotypes; two-way ANOVA P = 0.44 and P = 0.48, respectively. The numbers of fibers included in the analysis can be found in Table 2. All means ± SEM.

protein is found in almost all sensory neurons of the DRG (Hong et al., 2016), we chose to first evaluate whether loss of TMEM150C is associated with a quantitative change in the receptor properties of cutaneous sensory fibers, which make up the majority of the DRG. We used an ex vivo skin nerve preparation to record from single identified mechanoreceptors and nociceptors in the saphenous nerve using recording and stimulation protocols previously described (Schwaller et al., 2021; Walcher et al., 2018; Milenkovic et al., 2008). In total we made recordings from over 100 single fibers in WT and *Tmem150c*$^{LacZ/LacZ}$ mice (Table 1). The proportions of Aβ-fibers that could be classified as rapidly adapting mechanoreceptors (RAMs) or slowly adapting mechanoreceptors (SAMs) was unchanged in *Tmem150c*$^{lacZ/LacZ}$ mice compared to controls. Evaluation of the stimulus response properties of both mechanoreceptors and nociceptors revealed no significant differences between the two genotypes (Fig. S1). These negative results led us to evaluate whether there had been efficient ablation of the *Tmem150c* gene in this mutant mouse. TMEM150C is widely expressed, but public gene expression databases indicated that it is especially strongly expressed in epididymal tissue (Yue et al., 2014). Under ideal circumstances staining for β-galactosidase activity should reveal the cells that endogenously express the *Tmem150c* transcript in *Tmem150c*$^{LacZ/LacZ}$ mice. Indeed, we could observe robust β-galactosidase expression in the cells of the epididymis; however, we were never able to detect a signal in

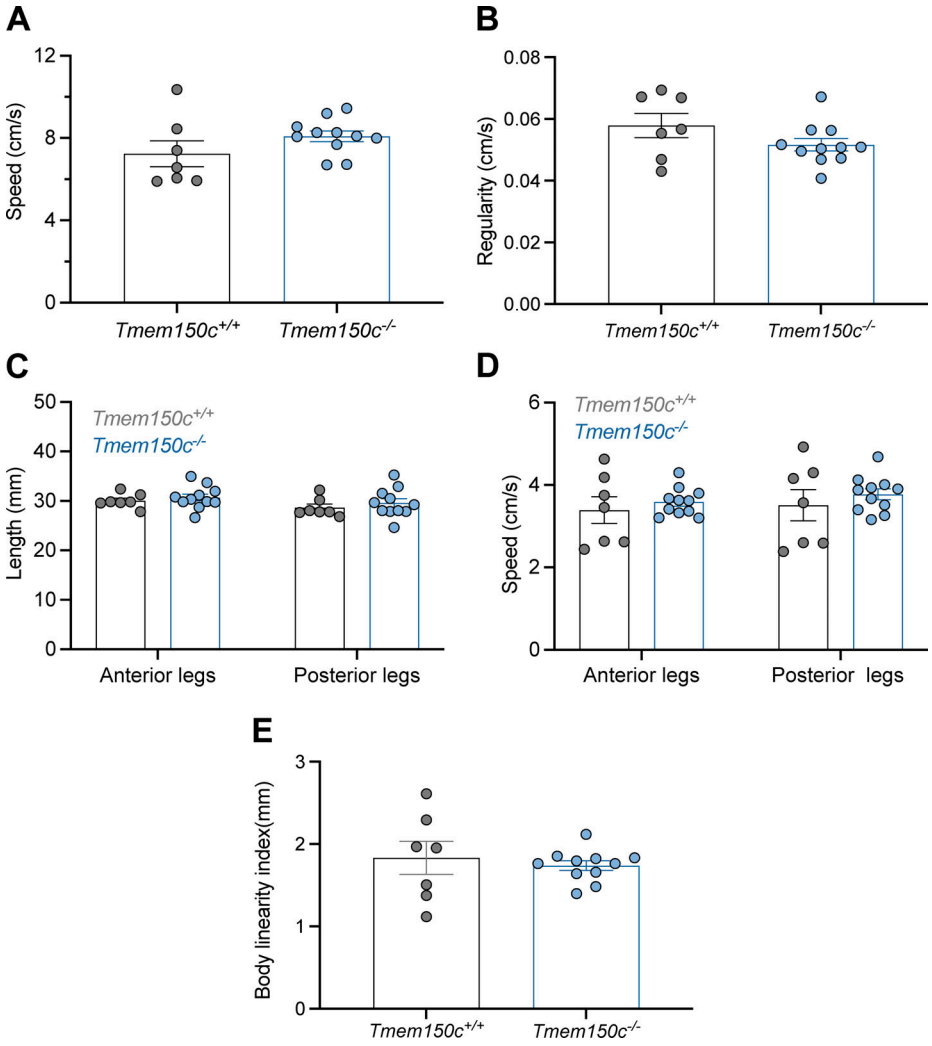

Figure 6. **Mouse walk behavior test shows comparable motor coordination in *Tmem150c*$^{-/-}$ and *Tmem150c*$^{+/+}$ mice. (A)** Average speed of each mouse from one end of the walkway to the other, showing no differences between *Tmem150c*$^{+/+}$ mice (7.24 ± 0.62) and *Tmem150c*$^{-/-}$ (8.09 ± 0.25) mice. Mann-Whitney test, P = 0.12. **(B)** Regularity of swing time for all legs was similar in *Tmem150c*$^{+/+}$ mice (0.05 ± 0.003) and *Tmem150c*$^{-/-}$ mice (0.05 ± 0.002). Mann-Whitney test, P = 0.25. **(C)** No differences were observed in step distance between each swing in control *Tmem150c*$^{+/+}$ and *Tmem150c*$^{-/-}$ mice; anterior legs (WT, 30.05 ± 0.54; KO, 30.70 ± 0.68; Mann-Whitney, P = 0.37) and posterior legs (WT, 28.64 ± 0.70; KO, 29.60 ± 0.87; Mann-Whitney, P = 0.21). **(D)** Swing speed average for individual steps from the anterior (WT, 3.38 ± 0.32; KO, 3.58 ± 0.10; Mann-Whitney, P = 0.72) and posterior legs (WT, 3.50 ± 0.37; KO, 3.77 ± 0.13; Mann-Whitney, P = 0.79) were comparable between *Tmem150c*$^{+/+}$ and *Tmem150c*$^{-/-}$ mice. **(E)** No differences were observed in the body linearity index in *Tmem150c*$^{+/+}$ (1.83 ± 0.19) and *Tmem150c*$^{-/-}$ mice (1.74 ± 0.19); Mann-Whitney test, P = 0.66. Data expressed as mean ± SEM.

sections taken from the DRG (Fig. 2 B). This prompted us to ask whether there was splicing around the β-galactosidase neomycin cassette in sensory neurons. Using RT-PCR for an amplicon located in the *Tmem150c* transcript downstream of the intronic neomycin insertion, we could indeed amplify a PCR product in the DRG, but not in the epididymis of *Tmem150c*$^{LacZ/LacZ}$ mice (Fig. 2 C). We cloned and sequenced the amplicon amplified from the DRGs of *Tmem150c*$^{LacZ/LacZ}$ mice and could confirm that the sequence was identical to the mature *Tmem150c* transcript. Thus, at least some full-length transcripts encoding the TMEM150C protein is present in the DRGs of *Tmem150c*$^{LacZ/LacZ}$ mice. These data indicated that the genetic strategy for ablating the *Tmem150c* gene using the knockout-first allele may not lead to complete ablation of TMEM150c at least in sensory neurons.

In order to reliably examine the functional importance of TMEM150C in sensory neurons, we generated another allele in which the *Tmem150c* locus was ablated using a CRISPR/Cas9 gene-editing strategy (Fig. 2 D). In this strategy, a genomic region encompassing Exon2–Exon5 was excised so that the sequences encoding transmembrane domains 1–2 were deleted followed by a frameshift. We obtained live heterozygous mice with this allele which we show is a true null allele (*Tmem150c*$^{-/-}$). We were able to generate *Tmem150c*$^{-/-}$ mice which also appeared viable and healthy, like *Tmem150c*$^{LacZ/lacZ}$ mice. We could confirm expression of the TMEM150c protein in WT mouse DRGs using Western blotting which revealed a specific protein band with an apparent molecular weight of ∼25 kD as predicted from the amino acid sequence. Importantly the TMEM150c protein

band was completely absent from the DRG of *Tmem150c*$^{-/-}$ mice, confirming that these mice are true null mutants (Fig. 2 F). We also performed immunocytochemistry for TMEM150C on sections of the DRG taken from WT and *Tmem150c*$^{-/-}$ mice. Although DRG neuronal cell bodies appeared to be positive for TMEM150C, this staining was indistinguishable from that found in DRGs from *Tmem150c*$^{-/-}$ mice (Fig. 2 G). It is possible that loss of TMEM150C may affect the development or anatomical integrity of the peripheral nervous system. We thus made an anatomical assessment of the peripheral nerves of WT and *Tmem150c*$^{-/-}$ mutant mice. Using transmission electron microscopy, we examined the ultrastructure of sensory axons in the tibial nerve and found normal large and thinly myelinated axons. We calculated the G-ratios for the myelin sheath which was not different between WT *Tmem150c*$^{-/-}$ mice. Unmyelinated fibers present in Remak bundles also had normal morphologies in *Tmem150c*$^{-/-}$ mice. Finally, we counted the numbers of myelinated and unmyelinated axons in the peripheral nerve and found no evidence of axonal loss in *Tmem150c*$^{-/-}$ mice (Fig. 3).

Although TMEM150c seems unlikely to be able to form a mechanosensitive ion channel by itself (Fig. 1), it may have an important modulatory function on components of the mechanotransduction apparatus in sensory neurons. We thus examined in detail the physiological properties of mechanoreceptors and nociceptors in the tibial nerve that innervate the glabrous skin of the mouse hindlimb in WT and *Tmem150c*$^{-/-}$ mice using established methodology (Walcher et al., 2018; Schwaller et al., 2021). We recorded from at least 40 single Aβ-fiber mechanoreceptors in each genotype and noted no change in the proportion of fibers that could be classified as RAMs or SAMs (Table 2). Two types of mechanoreceptors, Aβ-fiber RAMs and Aδ-fiber D-hair receptors, only respond to moving mechanical stimuli and show distinctive velocity sensitivity that can be measured using a series of ramp stimuli with increasing velocity (Heidenreich et al., 2012; Walcher et al., 2018; Schwaller et al., 2021). RAMs and D-hair receptors in *Tmem150c*$^{-/-}$ had typically low mechanical thresholds that did not differ from those in WT mice (Fig. 4, A and B). The velocity sensitivity of these two mechanoreceptors were also indistinguishable between WT and *Tmem150c*$^{-/-}$ mice (Fig. 4, C and D). In their initial studies, Hong and colleagues claimed that TMEM150C could mediate a mechanosensitive current with slow inactivation. Almost all mechanoreceptors display so-called RA-mechanosensitive currents that inactivate in <5 ms (Hu and Lewin, 2006; Lechner and Lewin, 2013; Lechner et al., 2009). It is thus possible that lack of TMEM150C has no effect of mechanoreceptors that normally only display RA-mechanosensitive currents. However, a small proportion of presumptive mechanoreceptors and a large proportion of nociceptors display intermediate or slowly adapting mechanosensitive currents (Hu and Lewin, 2006; Lechner et al., 2009; Lechner and Lewin, 2009; Coste et al., 2007). We thus targeted populations of cutaneous sensory neurons that might exhibit slower inactivating mechanosensitive currents. We recorded from both myelinated and unmyelinated cutaneous nociceptors in control and *Tmem150c*$^{-/-}$ mice (Table 2). We used a series of ramp and hold mechanical stimuli to probe their stimulus response properties. SAMs in the glabrous skin innervate Merkel cell complexes and are both velocity sensitive and respond tonically to small static forces. We also found that the velocity sensitivity and static force sensitivity of SAMs in *Tmem150c*$^{-/-}$ mice were statistically indistinguishable from those recorded in WT mice (Fig. 4, E–G).

We measured the force required to evoke the first spike during the ramp of the stimulus (Fig. 5 A) and found that for AMs the mean threshold for activation in *Tmem150c*$^{-/-}$ mutant mice was almost identical to those measured from WT (Fig. 5 B). The stimulus response function of AMs in WT and *Tmem150c*$^{-/-}$ mice were also not different (Fig. 5 C). We divided C-fiber nociceptors into those that only respond to mechanical stimuli and do not respond to heating and cooling stimuli, so-called C-mechanonociceptors (CMs) and Polymodal nociceptors, which respond to mechanical and thermal stimuli. These two types of nociceptors have different stimulus response properties to mechanical force (examples in Fig. 5 A; Milenkovic et al., 2008). Neither C-Ms nor Polymodal nociceptors showed different mean force thresholds or stimulus response properties in *Tmem150c*$^{-/-}$ mice compared to controls (Fig. 5, D–G). We conclude that the mechanosensory properties of virtually all types of cutaneous sensory neurons were unaffected in the absence of TMEM150C.

In their original paper, examining mice with a *Tmem150c* allele generated through the knockout first strategy, Hong and colleagues described a deficit in motor coordination in these mice that they attributed to changes in proprioceptor properties (Hong et al., 2016). We did not notice any overt motor coordination deficits in *Tmem150c*$^{-/-}$ mice, but decided to quantify motor behavior using a so-called catwalk assay (Mendes et al., 2015). We analyzed various gait parameters such as locomotion speed, regularity of swing phase and step distances and could not detect any significant deficits in *Tmem150c*$^{-/-}$ mice compared to WT controls (Fig. 6).

Discussion

The membrane protein TMEM150C or Tentonin3 has been proposed to form a mechanosensitive ion channel in proprioceptors, nodose neurons innervating the aortic arch (Lu et al., 2020) and even in pancreatic β cells (Wee et al., 2021). However, early follow-up studies could not reproduce the finding that heterologous expression of *Tmem150c* is associated with the appearance of mechanosensitive currents, when PIEZO1 channels are absent (Anderson et al., 2018; Dubin et al., 2017). Here, we could confirm that the expression of *Tmem150c* in N2a cells lacking PIEZO1 channels is not associated with the appearance of indentation evoked currents. In addition, we could show that two further modes of stimulation that efficiently activate mechanosensitive channels, membrane stretch and substrate deflection, also do not evoke currents in cells expressing *Tmem150c* (Fig. 1). Using a knockout mouse model, it has been claimed that loss of the TMEM150C protein is associated with a loss of mechanosensitive currents with slow inactivation kinetics in DRG neurons, nodose neurons, and pancreatic β-cells (Hong et al., 2016; Lu et al., 2020; Wee et al., 2021). Here, we used the same mouse model, but found that the knockout-first gene targeting strategy was associated with remaining mature WT

Tmem150c transcripts in the DRG (Fig. 2). We could also not detect β-galactosidase activity in the DRG which should be present in cells in which the gene has been effectively silenced. We concluded that the *Tmem150c*$^{lacZ/lacZ}$ mice may not produce a complete gene ablation at least in some tissues. In order to better test for a possible function of TMEM150C in vivo, we created a new mouse model in which a large part of the *Tmem150c* locus was ablated. This new *Tmem150c*$^{-/-}$ mouse was viable and seemingly healthy. Even if TMEM150C forms an accessory subunit of mechanosensitive ion channels then it would seem likely that sensory neurons in *Tmem150c*$^{-/-}$ mice would show physiological deficits. We made extensive single-unit recordings from cutaneous sensory neurons from WT and *Tmem150c*$^{-/-}$ mutant mice. We detected no deficits in the mechanosensitivity of sensory neurons lacking TMEM150C. If *Tmem150c*$^{-/-}$ mutant mice have strongly reduced proprioceptor function, we might expect to observe deficits in locomotor behavior. However, an analysis of the gait of *Tmem150c*$^{-/-}$ mutant mice revealed that these animals have normal gait parameters indistinguishable from WT mice. We conclude that there is little or no evidence that the TMEM150C protein participates in sensory mechanotransduction.

Most of the evidence gathered for a functional role of TMEM150C in mediating endogenous slowly inactivating mechanosensitive currents relies on the use of the *Tmem150c*$^{lacZ/LacZ}$ mouse model (Lu et al., 2020; Hong et al., 2016; Wee et al., 2021). Here, we show that *Tmem150c*$^{lacZ/LacZ}$ mice may carry a hypomorphic mutation that allows expression of WT *Tmem150c* in some tissues. The wide range of phenotypes described in this mouse model should therefore be treated with some caution. It is known that insertion of genetic elements into introns which is a necessary part of the knockout first strategy (Tate and Skarnes, 2011) may lead to unexpected effects even on the expression of unrelated genes (Pan et al., 2016). In the published studies using the *Tmem150c*$^{lacZ/LacZ}$ mouse model, there was no examination of LacZ activity in the cell types studied with reduced mechanosensitive currents. Furthermore, proof of the success of the gene deletion appeared to be solely based on lack of immunopositive cells in *Tmem150c*$^{lacZ/LacZ}$ tissues (Wee et al., 2021; Lu et al., 2020; Hong et al., 2016). We used antibodies directed against the same epitope described in Hong et al. (2016) to detect the protein in WT DRG sections and in sections from *Tmem150c*$^{-/-}$ mice. Unfortunately, in our hands, we always observed a substantial background staining in DRG sections taken from *Tmem150c*$^{-/-}$ mice using such antibodies (Fig. 2).

Here, we used the *Tmem150c*$^{-/-}$ mutant mice to try and definitively answer the question of whether TMEM150C has a nonredundant function in sensory neurons of the DRG. It is clear that TMEM150C is found in many DRG neurons (Hong et al., 2016; Parpaite et al., 2021; Usoskin et al., 2015), but recent experiments have also cast doubt on whether the presence of TMEM150C is required for the expression of mechanosensitive currents in cultured sensory neurons (Parpaite et al., 2021). Additionally, there is now evidence that sensory neuron mechanosensitivity may not be solely dependent on channels within the sensory cell membrane. Thus, recently identified specialized Schwann cells that surround the peripheral endings of unmyelinated nociceptors may directly participate in the detection of noxious mechanical stimuli (Abdo et al., 2019; Ojeda-Alonso et al., 2022 *Preprint*). In addition, cells that form specialized sensory end-organs innervated by mechanoreceptors in birds were also recently shown to be mechanosensitive (Nikolaev et al., 2020). Using our global *Tmem150c*$^{-/-}$ mutant mice, we wished to test whether loss of the TMEM150C protein had an impact on the mechanosensitive properties of functionally identified sensory neurons using ex vivo skin nerve preparations. Recordings from identified sensory neuron populations has in the past proved a reliable way to reveal physiological deficits in mice lacking genes that participate in sensory mechanotransduction or regulate excitability (Heidenreich et al., 2012; Wang and Lewin, 2011; Ranade et al., 2014; Wetzel et al., 2007; Ventéo et al., 2016; Schwaller et al., 2021; Dawes et al., 2018; Murthy et al., 2018). We reasoned that we should observe some deficits in defined sensory neuron types if TMEM150C is required for the expression of slowly inactivating currents in sensory neurons or in sensory Schwann cells. Instead, here we detected no change in the physiological properties of identified nociceptors and mechanoreceptors in mice lacking TMEM150C. It is of course conceivable that we did not observe deficits because the effect was subtle or found in a rare subtype of mechanoreceptor that was not adequately sampled. In the experiments described here, we only characterized the receptor properties of neurons which were first identified with mechanical search stimulus. Sensory fibers lacking a mechanosensitive receptive field, like those found in *Stoml3*$^{-/-}$ or *Piezo2*$^{-/-}$ mutant mice, could have been missed in this study. However, in mutant mice with such a profound mechanosensory deficit, we always found deficits in the stimulus response properties of remaining afferent populations (Wetzel et al., 2007; Ranade et al., 2014; Murthy et al., 2018). In their original paper, Hong and colleagues claimed to observe deficits in the muscle stretch-activated activity of muscle afferents innervating the extensor digitorum longus muscle in the hind limb (Hong et al., 2016). In their study, Hong and colleagues recorded afferent multiunit activity from the whole nerve (Hong et al., 2016), but did not identify and classify functional subtypes of muscle afferents (Lewin and McMahon, 1991). Here, we did not attempt to make a detailed analysis of identified muscle afferents as we did not observe any deficits in gait parameters (Fig. 6).

In summary, we have provided comprehensive evidence that TMEM150C does not by itself form a mechanosensitive ion channel. Furthermore, we show that in animals with a true homozygous null mutation of the *Tmem150c* locus there is no indication of any physiological deficits in any of the major physiologically defined mechanoreceptor and nociceptor populations that innervate the skin. We conclude that it is unlikely that the TMEM150C protein is a necessary regulator of mechanosensitive ion channels that are required for the normal function of somatosensory neurons.

Data availability

All data is available in the main text or the supplementary materials. All data, code, and materials used in the analysis are available upon request.

Acknowledgments

Crina M. Nimigean served as editor.

We thank the EM core facility staff Dr. Séverine Kunz and Christina Schiel for their contribution. We thank members of the Lewin lab for constructive comments on the manuscript. Technical assistance was provided by Maria Braunschweig, Kathleen Barda, Franziska Bartelt, and Nadine Groβ.

This research was funded by the European Research Council and the Deutsche Forschungsgemeinschaft (Sensational Tethers 789128 to G.R. Lewin; SFB 958 Project A9).

The authors declare no competing financial interests.

Author contributions: Conceptualization: J. Ojeda-Alonso, G.R. Lewin, and V. Bégay; mouse models/experimental design: V. Bégay, G.R. Lewin, and J. Ojeda-Alonso; nerve recording and formal analysis: J. Ojeda-Alonso: mouse behavior J. Ojeda-Alonso and J.A. Garcia-Contreras; patch clamp electrophysiology: J. Ojeda-Alonso and J.A. Garcia-Contreras; electron microscopy: B. Purfürst, J. Ojeda-Alonso, A.F. Campos-Pérez, and V. Bégay; writing G.R. Lewin and J. Ojeda-Alonso with input from all authors. Supervision and funding: G.R. Lewin.

Submitted: 30 January 2022
Accepted: 28 September 2022

References

Abdo, H., L. Calvo-Enrique, J.M. Lopez, J. Song, M.-D. Zhang, D. Usoskin, A. El Manira, I. Adameyko, J. Hjerling-Leffler, and P. Ernfors. 2019. Specialized cutaneous Schwann cells initiate pain sensation. *Science*. 365: 695–699. https://doi.org/10.1126/science.aax6452

Anderson, E.O., E.R. Schneider, J.D. Matson, E.O. Gracheva, and S.N. Bagriantsev. 2018. TMEM150C/Tentonin3 is a regulator of mechano-gated ion channels. *Cell Rep.* 23:701–708. https://doi.org/10.1016/j.celrep.2018.03.094

Arnadóttir, J., and M. Chalfie. 2010. Eukaryotic mechanosensitive channels. *Annu. Rev. Biophys.* 39:111–137. https://doi.org/10.1146/annurev.biophys.37.032807.125836

Brown, A.L., Z. Liao, and M.B. Goodman. 2008. MEC-2 and MEC-6 in the *Caenorhabditis elegans* sensory mechanotransduction complex: Auxiliary subunits that enable channel activity. *J. Gen. Physiol.* 131:605–616. https://doi.org/10.1085/jgp.200709910

Chelur, D.S., G.G. Ernstrom, M.B. Goodman, C.A. Yao, L. Chen, R. O' Hagan, and M. Chalfie. 2002. The mechanosensory protein MEC-6 is a subunit of the *C. elegans* touch-cell degenerin channel. *Nature*. 420:669–673. https://doi.org/10.1038/nature01205

Chesler, A.T., M. Szczot, D. Bharucha-Goebel, M. Čeko, S. Donkervoort, C. Laubacher, L.H. Hayes, K. Alter, C. Zampieri, C. Stanley, et al. 2016. The role of PIEZO2 in human mechanosensation. *N. Engl. J. Med.* 375: 1355–1364. https://doi.org/10.1056/NEJMoa1602812

Coste, B., M. Crest, and P. Delmas. 2007. Pharmacological dissection and distribution of NaN/Nav1.9, T-type Ca^{2+} currents, and mechanically activated cation currents in different populations of DRG neurons. *J. Gen. Physiol.* 129:57–77. https://doi.org/10.1085/jgp.200609665

Coste, B., J. Mathur, M. Schmidt, T.J. Earley, S. Ranade, M.J. Petrus, A.E. Dubin, and A. Patapoutian. 2010. Piezo1 and Piezo2 are essential components of distinct mechanically activated cation channels. *Science*. 330: 55–60. https://doi.org/10.1126/science.1193270

Dawes, J.M., G.A. Weir, S.J. Middleton, R. Patel, K.I. Chisholm, P. Pettingill, L.J. Peck, J. Sheridan, A. Shakir, L. Jacobson, et al. 2018. Immune or genetic-mediated disruption of CASPR2 causes pain hypersensitivity due to enhanced primary afferent excitability. *Neuron*. 97:806–822.e10. https://doi.org/10.1016/j.neuron.2018.01.033

Driscoll, M., and M. Chalfie. 1991. The mec-4 gene is a member of a family of *Caenorhabditis elegans* genes that can mutate to induce neuronal degeneration. *Nature*. 349:588–593. https://doi.org/10.1038/349588a0

Dubin, A.E., S. Murthy, A.H. Lewis, L. Brosse, S.M. Cahalan, J. Grandl, B. Coste, and A. Patapoutian. 2017. Endogenous Piezo1 can confound mechanically activated channel identification and characterization. *Neuron*. 94:266–270.e3. https://doi.org/10.1016/j.neuron.2017.03.039

Goodman, M.B., G.G. Ernstrom, D.S. Chelur, R. O'Hagan, C.A. Yao, and M. Chalfie. 2002. MEC-2 regulates *C. elegans* DEG/ENaC channels needed for mechanosensation. *Nature*. 415:1039–1042. https://doi.org/10.1038/4151039a

Heidenreich, M., S.G. Lechner, V. Vardanyan, C. Wetzel, C.W. Cremers, E.M. De Leenheer, G. Aránguez, M.Á. Moreno-Pelayo, T.J. Jentsch, and G.R. Lewin. 2011. KCNQ4 K(+) channels tune mechanoreceptors for normal touch sensation in mouse and man. *Nat. Neurosci.* 15:138–145. https://doi.org/10.1038/nn.2985

Herget, R. 2015. Identification of sensory neuron membrane proteins with a role in mechanotransduction. Freie Universität, Berlin.

Hoffman, B.U., Y. Baba, S.A. Lee, C.-K. Tong, E.E. Konofagou, and E.A. Lumpkin. 2022. Focused ultrasound excites action potentials in mammalian peripheral neurons in part through the mechanically gated ion channel PIEZO2. *Proc. Natl. Acad. Sci. USA*. 119:e2115821119. https://doi.org/10.1073/pnas.2115821119

Hong, G.-S., B. Lee, J. Wee, H. Chun, H. Kim, J. Jung, J.Y. Cha, T.-R. Riew, G.H. Kim, I.-B. Kim, and U. Oh. 2016. Tentonin 3/TMEM150c confers distinct mechanosensitive currents in dorsal-root ganglion neurons with proprioceptive function. *Neuron*. 91:708–710. https://doi.org/10.1016/j.neuron.2016.07.019

Hu, J., and G.R. Lewin. 2006. Mechanosensitive currents in the neurites of cultured mouse sensory neurones. *J. Physiol.* 577:815–828. https://doi.org/10.1113/jphysiol.2006.117648

Huang, M., G. Gu, E.L. Ferguson, and M. Chalfie. 1995. A stomatin-like protein necessary for mechanosensation in *C. elegans*. *Nature*. 378:292–295. https://doi.org/10.1038/378292a0

Lechner, S.G., H. Frenzel, R. Wang, and G.R. Lewin. 2009. Developmental waves of mechanosensitivity acquisition in sensory neuron subtypes during embryonic development. *EMBO J.* 28:1479–1491. https://doi.org/10.1038/emboj.2009.73

Lechner, S.G., and G.R. Lewin. 2009. Peripheral sensitisation of nociceptors via G-protein-dependent potentiation of mechanotransduction currents. *J. Physiol.* 587:3493–3503. https://doi.org/10.1113/jphysiol.2009.175059

Lechner, S.G., and G.R. Lewin. 2013. Hairy sensation. *Physiology*. 28:142–150. https://doi.org/10.1152/physiol.00059.2012

Lewin, G.R., and S.B. McMahon. 1991. Physiological properties of primary sensory neurons appropriately and inappropriately innervating skeletal muscle in adult rats. *J. Neurophysiol.* 66:1218–1231. https://doi.org/10.1152/jn.1991.66.4.1218

Lobe, C.G., K.E. Koop, W. Kreppner, H. Lomeli, M. Gertsenstein, and A. Nagy. 1999. Z/AP, a double reporter for cre-mediated recombination. *Dev. Biol.* 208:281–292. https://doi.org/10.1006/dbio.1999.9209

Lu, H.-J., T.-L. Nguyen, G.-S. Hong, S. Pak, H. Kim, H. Kim, D.-Y. Kim, S.-Y. Kim, Y. Shen, P.D. Ryu, et al. 2020. Tentonin 3/TMEM150C senses blood pressure changes in the aortic arch. *J. Clin. Invest.* 130:3671–3683. https://doi.org/10.1172/JCI133798

Mendes, C.S., I. Bartos, Z. Márka, T. Akay, S. Márka, and R.S. Mann. 2015. Quantification of gait parameters in freely walking rodents. *BMC Biol.* 13:50. https://doi.org/10.1186/s12915-015-0154-0

Milenkovic, N., C. Wetzel, R. Moshourab, and G.R. Lewin. 2008. Speed and temperature dependences of mechanotransduction in afferent fibers recorded from the mouse saphenous nerve. *J. Neurophysiol.* 100: 2771–2783. https://doi.org/10.1152/jn.90799.2008

Moroni, M., M.R. Servin-Vences, R. Fleischer, O. Sánchez-Carranza, and G.R. Lewin. 2018. Voltage gating of mechanosensitive PIEZO channels. *Nat. Commun.* 9:1096. https://doi.org/10.1038/s41467-018-03502-7

Murthy, S.E., M.C. Loud, I. Daou, K.L. Marshall, F. Schwaller, J. Kühnemund, A.G. Francisco, W.T. Keenan, A.E. Dubin, G.R. Lewin, and A. Patapoutian. 2018. The mechanosensitive ion channel Piezo2 mediates sensitivity to mechanical pain in mice. *Sci. Transl. Med.* 10:eaat9897. https://doi.org/10.1126/scitranslmed.aat9897

Nikolaev, Y.A., V.V. Feketa, E.O. Anderson, E.R. Schneider, E.O. Gracheva, and S.N. Bagriantsev. 2020. Lamellar cells in Pacinian and Meissner corpuscles are touch sensors. *Sci. Adv.* 6:eabe6393. https://doi.org/10.1126/sciadv.abe6393

O'Hagan, R., M. Chalfie, and M.B. Goodman. 2005. The MEC-4 DEG/ENaC channel of *Caenorhabditis elegans* touch receptor neurons transduces mechanical signals. *Nat. Neurosci.* 8:43–50. https://doi.org/10.1038/nn1362

Ojeda-Alonso, J., L. Calvo-Enrique, R. Paricio-Montesinos, R. Kumar, M.-D. Zhang, J.F.A. Poulet, P. Ernfors, and G.R. Lewin. 2022. Sensory

Schwann cells are required for mechanical nociception and touch perception. *bioRxiv*. (Preprint posted February 04, 2022). https://doi.org/10.1101/2022.02.04.477749

Omerbašić, D., L.-N. Schuhmacher, Y.-A. Bernal Sierra, E.S.J. Smith, and G.R. Lewin. 2015. ASICs and mammalian mechanoreceptor function. *Neuropharmacology*. 94:80–86. https://doi.org/10.1016/j.neuropharm.2014.12.007

Pan, Y., L. Zhang, Q. Liu, Y. Li, H. Guo, Y. Peng, H. Peng, B. Tang, Z. Hu, J. Zhao, et al. 2016. Insertion of a knockout-first cassette in Ampd1 gene leads to neonatal death by disruption of neighboring genes expression. *Sci. Rep.* 6:35970. https://doi.org/10.1038/srep35970

Parpaite, T., L. Brosse, N. Séjourné, A. Laur, Y. Mechioukhi, P. Delmas, and B. Coste. 2021. Patch-seq of mouse DRG neurons reveals candidate genes for specific mechanosensory functions. *Cell Rep.* 37:109914. https://doi.org/10.1016/j.celrep.2021.109914

Patkunarajah, A., J.H. Stear, M. Moroni, L. Schroeter, J. Blaszkiewicz, J.L. Tearle, C.D. Cox, C. Fuerst, O. Sánchez-Carranza, M.D.Á.O. Fernández, et al. 2020. TMEM87a/Elkin1, a component of a novel mechanoelectrical transduction pathway, modulates melanoma adhesion and migration. *eLife*. 9:e53308. https://doi.org/10.7554/eLife.53308

Poole, K., R. Herget, L. Lapatsina, H.-D. Ngo, and G.R. Lewin. 2014a. Tuning Piezo ion channels to detect molecular-scale movements relevant for fine touch. *Nat. Commun.* 5:3520. https://doi.org/10.1038/ncomms4520

Poole, K., M. Moroni, and G.R. Lewin. 2015. Sensory mechanotransduction at membrane-matrix interfaces. *Pflugers Arch.* 467:121–132. https://doi.org/10.1007/s00424-014-1563-6

Ranade, S.S., S.-H. Woo, A.E. Dubin, R.A. Moshourab, C. Wetzel, M. Petrus, J. Mathur, V. Bégay, B. Coste, J. Mainquist, et al. 2014. Piezo2 is the major transducer of mechanical forces for touch sensation in mice. *Nature*. 516:121–125. https://doi.org/10.1038/nature13980

Schwaller, F., V. Bégay, G. García-García, F.J. Taberner, R. Moshourab, B. McDonald, T. Docter, J. Kühnemund, J. Ojeda-Alonso, R. Paricio-Montesinos, et al. 2021. USH2A is a Meissner's corpuscle protein necessary for normal vibration sensing in mice and humans. *Nat. Neurosci.* 24:74–81. https://doi.org/10.1038/s41593-020-00751-y

Servin-Vences, M.R., M. Moroni, G.R. Lewin, and K. Poole. 2017. Direct measurement of TRPV4 and PIEZO1 activity reveals multiple mechanotransduction pathways in chondrocytes. *Elife*. 6:e21074. https://doi.org/10.7554/eLife.21074

Smith, E.S.J., B. Purfürst, T. Grigoryan, T.J. Park, N.C. Bennett, and G.R. Lewin. 2012. Specific paucity of unmyelinated C-fibers in cutaneous peripheral nerves of the african naked-mole rat: Comparative analysis using six species of bathyergidae. *J. Comp. Neurol.* 520:2785–2803. https://doi.org/10.1002/cne.23133

Szczot, M., J. Liljencrantz, N. Ghitani, A. Barik, R. Lam, J.H. Thompson, D. Bharucha-Goebel, D. Saade, A. Necaise, S. Donkervoort, et al. 2018. PIEZO2 mediates injury-induced tactile pain in mice and humans. *Sci. Transl. Med.* 10:eaat9892. https://doi.org/10.1126/scitranslmed.aat9892

Taberner, F.J., V. Prato, I. Schaefer, K. Schrenk-Siemens, P.A. Heppenstall, and S.G. Lechner. 2019. Structure-guided examination of the mechanogating mechanism of PIEZO2. *Proc. Natl. Acad. Sci. USA*. 116:14260–14269. https://doi.org/10.1073/pnas.1905985116

Tate, P.H., and W.C. Skarnes. 2011. Bi-allelic gene targeting in mouse embryonic stem cells. *Methods*. 53:331–338. https://doi.org/10.1016/j.ymeth.2010.12.025

Usoskin, D., A. Furlan, S. Islam, H. Abdo, P. Lönnerberg, D. Lou, J. Hjerling-Leffler, J. Haeggström, O. Kharchenko, P.V. Kharchenko, et al. 2015. Unbiased classification of sensory neuron types by large-scale single-cell RNA sequencing. *Nat. Neurosci.* 18:145–153. https://doi.org/10.1038/nn.3881

Ventéo, S., S. Laffray, C. Wetzel, C. Rivat, F. Scamps, I. Méchaly, L. Bauchet, C. Raoul, E. Bourinet, G.R. Lewin, et al. 2016. Fxyd2 regulates Aδ- and C-fiber mechanosensitivity and is required for the maintenance of neuropathic pain. *Sci. Rep.* 6:36407. https://doi.org/10.1038/srep36407

Walcher, J., J. Ojeda-Alonso, J. Haseleu, M.K. Oosthuizen, A.H. Rowe, N.C. Bennett, and G.R. Lewin. 2018. Specialized mechanoreceptor systems in rodent glabrous skin. *J. Physiol.* 596:4995–5016. https://doi.org/10.1113/JP276608

Wang, R., and G.R. Lewin. 2011. The Cav3.2 T-type calcium channel regulates temporal coding in mouse mechanoreceptors. *J. Physiol.* 589:2229–2243. https://doi.org/10.1113/jphysiol.2010.203463

Wee, J., S. Pak, T. Kim, G.-S. Hong, J.S. Lee, J. Nan, H. Kim, M.-O. Lee, K.S. Park, and U. Oh. 2021. Tentonin 3/TMEM150C regulates glucose-stimulated insulin secretion in pancreatic β-cells. *Cell Rep.* 37:110067. https://doi.org/10.1016/j.celrep.2021.110067

Wetzel, C., J. Hu, D. Riethmacher, A. Benckendorff, L. Harder, A. Eilers, R. Moshourab, A. Kozlenkov, D. Labuz, O. Caspani, et al. 2007. A stomatin-domain protein essential for touch sensation in the mouse. *Nature*. 445:206–209. https://doi.org/10.1038/nature05394

Wetzel, C., S. Pifferi, C. Picci, C. Gök, D. Hoffmann, K.K. Bali, A. Lampe, L. Lapatsina, R. Fleischer, E.S.J. Smith, et al. 2017. Small-molecule inhibition of STOML3 oligomerization reverses pathological mechanical hypersensitivity. *Nat. Neurosci.* 20:209–218. https://doi.org/10.1038/nn.4454

Yue, F., Y. Cheng, A. Breschi, J. Vierstra, W. Wu, T. Ryba, R. Sandstrom, Z. Ma, C. Davis, B.D. Pope, et al. 2014. A comparative encyclopedia of DNA elements in the mouse genome. *Nature*. 515:355–364. https://doi.org/10.1038/nature13992

Supplemental material

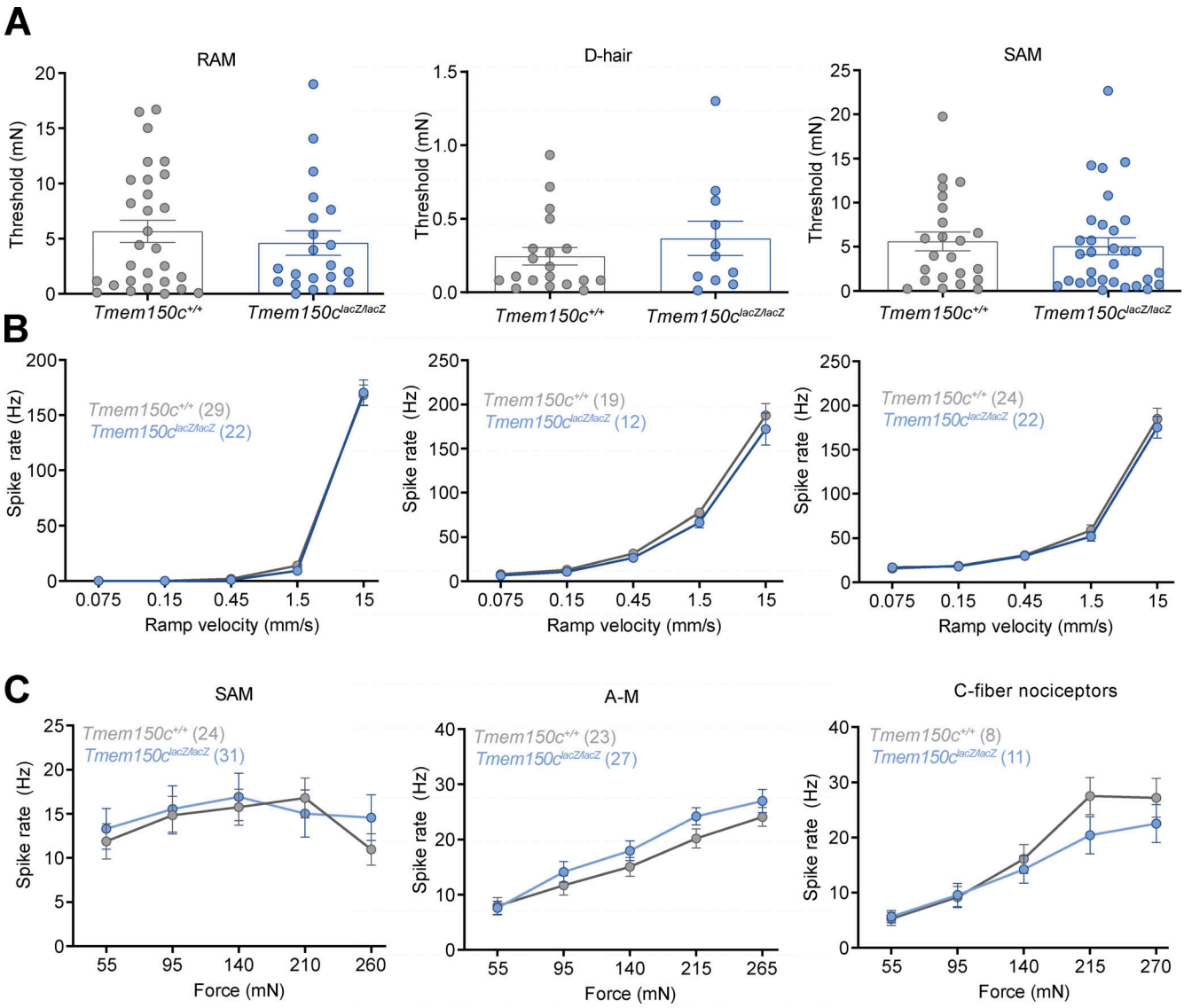

Figure S1. **Mechanoreceptors and nociceptors in the hairy skin of *Tmem150c*$^{lacZ/lacZ}$ mice were unchanged compared to controls. (A)** Mechanoreceptors and nociceptors are unchanged in TMEM150C$^{lacz/lacz}$ mice. We found no differences in the mechanical thresholds between of RAMs (Wilcoxin signed rank, P = 0.07), SAMs (Wilcoxin signed rank, P = 0.07), or D-hair receptors (Wilcoxin signed rank, P = 0.06) recorded from WT and *Tmem150c*$^{lacZ/LacZ}$ mice, data mean ± SEM. **(B)** The stimulus response functions of mechanoreceptors (RAMs, SAMs, and D-hair receptors) to moving ramp stimuli did not differ between WT and *Tmem150c*$^{lacZ/LacZ}$ mice; two-way ANOVA P = 0.82, P = 0.52, and P = 0.20, respectively; data are means ± SEM. **(C)** The responses of low threshold SAMs, high threshold AMs and C-fiber nociceptors to increasing ramp and hold forces did not change in *Tmem150c*$^{lacZ/LacZ}$ mice compared to WT; two-way ANOVA, P = 0.50, P = 0.21, and P = 0.14, respectively; data are means ± SEM.